The Plant Cell, Vol. 19: 1885–1897, June 2007, www.plantcell.org

INCREASED SIZE EXCLUSION LIMIT2 Encodes a Putative DEVH Box RNA Helicase Involved in Plasmodesmata Function during *Arabidopsis* Embryogenesis [W]

Ken Kobayashi,[a] Marisa S. Otegui,[b] Sujatha Krishnakumar,[c] Michael Mindrinos,[c] and Patricia Zambryski[a,1]

[a] Department of Plant and Microbial Biology, University of California, Berkeley, California 94720
[b] Department of Botany, University of Wisconsin, Madison, Wisconsin 53706-1381
[c] Stanford Genome Technology Center, Palo Alto, California 94304

Here, we characterize the *Arabidopsis thaliana* embryo-defective mutant *increased size exclusion limit2* (*ise2*). In contrast with wild-type embryos, *ise2* mutants continue to traffic 10-kD fluorescent dextran in the mid-torpedo stage of development. *ise2* embryos contain branched as well as simple plasmodesmata (PD) compared with wild-type embryos, which only contain simple PD. Positional cloning reveals that the *ISE2* gene encodes a putative DEVH box RNA helicase that shares sequence homology with RNA helicases involved in RNA degradation pathways in other organisms. ISE2 localizes to granule-like structures in the cytoplasm. These granules increase in number when plant cells are stressed. These features are characteristic of stress granules (SGs) in mammalian cells, suggesting that ISE2 granules represent plant-specific SGs. Genetic data demonstrate that the ISE2 helicase is involved in posttranscriptional gene silencing and the determination of cell fate. These data together suggest that ISE2 function affects PD structure and function through the regulation of RNA metabolism and consequent gene expression.

INTRODUCTION

Plant embryogenesis is a complex developmental process during which cell division and gene expression patterns are coordinated to establish the basic body plan of the organism. The morphological and developmental changes that take place during embryogenesis are well known (Berleth and Chatfield, 2002). However, the molecular and cellular mechanisms that underlie embryonic programming are not well understood. In *Arabidopsis thaliana*, it is estimated that at least 4000 essential genes need to be spatially and temporally regulated and finely coordinated during embryogenesis (Goldberg et al., 1989; West and Harada, 1993; Jurgens, 1995). To date, genetic studies have identified almost 350 genes affecting *Arabidopsis* embryogenesis (Tzafrir et al., 2004). Our laboratory is specifically interested in identifying genes, first expressed during embryogenesis, that are essential for intercellular communication.

Plant cells are encased in cell walls and are interconnected by dynamic intercellular channels termed plasmodesmata (PD) (reviewed in Roberts, 2005). The plasma membrane forms the outer limits of PD, and the desmotubule, derived from the endoplasmic reticulum (ER), forms the central axial core of PD. The space between the plasma membrane and the desmotubule provides a soluble conduit connecting the cytoplasm between adjacent cells. PD are essential gatekeepers for plant cell-to-cell transport and communication during all stages of plant growth, including embryogenesis. As PD have the innate ability to transport macromolecules, developmental transitions in PD function and aperture likely play critical roles in the transmission of macromolecular signals to coordinate differentiation pathways (Lee et al., 2003; Zambryski, 2004).

Ultrastructural observations suggest that all cells of the *Arabidopsis* embryo are connected by primary simple PD (Mansfield and Briarty, 1991). Consistent with observations in adult plants that less differentiated cells containing simple PD (such as sink tissues) have a larger PD aperture (Oparka et al., 1999; Crawford and Zambryski, 2000), embryonic simple PD allow increased cell-to-cell transport of macromolecules (such as 2X and 3X of 54 and 81 kD, respectively, green fluorescent protein [GFP]) compared with adult tissues (Kim et al., 2005a, 2005b). Detailed studies monitoring three different stages of embryogenesis indicated that different regions of the embryo body have distinct PD aperture defined as size exclusion limits (SELs), resulting in the formation of four symplastic subdomains by the mid-torpedo stage (Kim et al., 2005a, 2005b). These subdomains correspond to the basic plant body plan and include the shoot apex, cotyledons, hypocotyls, and root. Such studies predict that the regulation of the PD aperture is critical for embryonic patterning.

PD apertures/SELs fluctuate depending on physiology, development, and type of cell/tissue (Kobayashi et al., 2005). Previously, we determined that PD apertures are downregulated during embryogenesis (Kim et al., 2002). Fluorescently labeled (F) dextran tracers were introduced exogenously into embryos at different stages, and the extent of tracer cell-to-cell movement

[1] To whom correspondence should be addressed. E-mail zambrysk@nature.berkeley.edu; fax 510-642-4995.
The author responsible for distribution of materials integral to the findings presented in this article in accordance with the policy described in the Instructions for Authors (www.plantcell.org) is: Patricia Zambryski (zambrysk@nature.berkeley.edu).
[W] Online version contains Web-only data.
www.plantcell.org/cgi/doi/10.1105/tpc.106.045666

was evaluated. Early embryos (i.e., late-heart to early-torpedo stages) transport 10-kD F-dextran cell to cell, but PD aperture is downregulated at the torpedo stage so that wild-type mid-torpedo embryos no longer exhibit loading and cell-to-cell transport of 10-kD F-dextran. To identify genes that regulate PD aperture and function, embryo-defective lines were screened individually by fluorescence microscopy to identify mutants, called *increased size exclusion limit* (*ise*), that continued to traffic 10-kD F-dextran beyond mid-embryogenesis. This functional assay identified 15 *ise* mutant lines from 5000 embryo-defective lines screened (Kim et al., 2002).

Here, we present a detailed analysis of the *ise2* line, which is allelic to *emb25* (Franzmann et al., 1995) and maps to position 100 centimorgan on the lower arm of chromosome 1 (Kim et al., 2002). *ise2* mutants have a pleiotropic phenotype during embryogenesis and seedling development, including modification of embryonic PD ultrastructure and alterations in cell fate. Genetic data reveal that *ISE2* is required during posttranscriptional gene silencing (PTGS). The *ISE2* gene encodes a putative DEVH box RNA helicase sharing sequence homology with RNA helicases involved in RNA metabolism in other eukaryotes. ISE2 localizes to cytoplasmic granules that share features with one of the major classes of mRNA-containing granules in mammalian cells, called stress granules (SGs). The potential mechanism(s) of ISE2 function in the regulation of PD aperture/SEL is discussed.

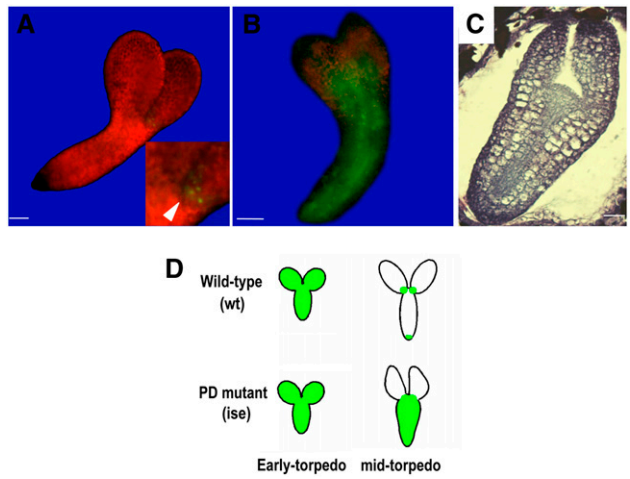

Figure 1. F-Dextran Loading of Wild-Type and *ise2* Mid-Torpedo Embryos.

(A) Partial loading at the base of a wild-type cotyledon is indicated by the arrowhead in the higher magnification shown in the boxed area.
(B) Green region shows 10-kD F-dextran in the hypocotyl of *ise2*.
(C) Longitudinal section of an *ise2* embryo stained with Safranin-O and Fast Green.
(D) Schematic representation of *Arabidopsis* embryo dye-loading assay. Bars = 50 μm in **(A)** and **(B)** and 20 μm in **(C)**.

RESULTS

Identification of the *ise2* Mutant by Screening for Altered Cell-to-Cell Transport

The *ise2* embryo mutant phenotype segregates as a single recessive trait, and since no unfertilized ovules were observed in *ISE2/ise2* heterozygote siliques, the *ISE2* gene acts after fertilization (Kim et al., 2002). Ninety percent of *ise2* mutant embryos continue to traffic 10-kD F-dextran after the mid-torpedo stage. As wild-type PD undergo a downregulation in aperture at this stage, leading to their inability to traffic 10-kD F-dextran, these results suggested that the *ise2* phenotype is correlated with an alteration in PD function that manifests in defective development. Alteration in PD-mediated cell-to-cell transport is not a general feature of embryo-defective lines, as the majority (>99%) of the embryo-defective lines we screened do not exhibit alterations in F-dextran transport (Kim et al., 2002).

ise2 development was compared with wild-type embryo development. Wild-type embryos turn green at the heart stage of embryogenesis, indicative of chloroplast development from proplastid progenitors (Schulz and Jensen, 1968; Mansfield and Briarty, 1991). Wild-type and *ISE2/ise2* heterozygous embryos remain green as their organs, such as hypocotyls and cotyledons, develop. The corresponding *ise2* embryos (from the same silique) were white by light microscopy and never turned green even at later stages, as generally occurs with embryo-lethal mutants (Yadegari et al., 1994). *ise2* embryos were reduced in size compared with wild-type embryos, and their cotyledons were smaller, with irregular borders, pointed tips, and uneven sizes (Figure 1). The slight red chlorophyll fluorescence seen in Figure 1B is due to image capture at high gain that is possible via fluorescence microscopy, confirming that *ise2* embryos produce very low levels of chlorophyll. *ise2* embryos have proportionally thicker hypocotyls and smaller cotyledons (see Supplemental Figure 1 online). However, the general organization of the tissues in the embryonic axis, such as procambial strands (see below), ground tissue, and protodermis, was indistinguishable from that of wild-type embryos described in the literature (Figure 1C) (Mansfield and Briarty, 1991). The *ise2* radicle and the shoot apical meristem (SAM) appeared normal but were often larger (see Supplemental Figure 1 online). *ise2* mutant embryos develop more slowly compared with wild-type embryos during the later stages of development. Abnormal morphology starts to be evident only after the heart stage. Figure 1D diagrams the 10-kD F-dextran loading assay.

ise2 seeds can germinate in vitro on agar plates containing Murashige and Skoog (MS) salt plus 1% sucrose, although the growth/developmental rate of *ise2* seedlings was slower compared with that of wild-type seedlings. Whereas wild-type seedlings displayed fully expanded green cotyledons, true leaves, and a well-developed root system by 14 d after germination, *ise2* seedlings were much smaller and white or pale green in color (Figure 2A). Underdeveloped cotyledons emerged from the *ise2* seeds but expanded very slowly and sometimes showed bumpy irregular surfaces and occasional anthocyanin expression (Figure 2B). Partial greening was observed in *ise2* seedlings only after culture for several weeks (Figure 2E). Most of the *ise2* seedlings developed leaf-like structures that were translucent and contained trichomes (Figures 2C and 2D). The aerial portions of the *ise2* seedlings generally were stunted and thicker and frequently exhibited callus-like structures after extended periods

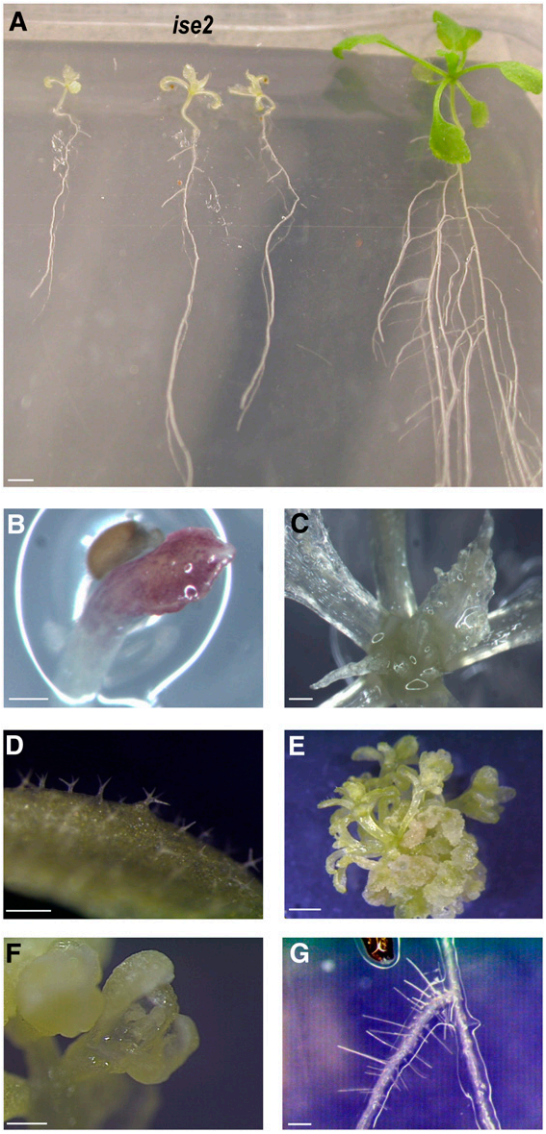

Figure 2. Phenotype of *ise2* Seedlings.

(A) *ise2* and wild-type seedlings germinated in MS medium + 1% sucrose at 2 weeks after germination.
(B) An *ise2* seedling cotyledon at 5 d after germination.
(C), **(D)**, and **(G)** SAM **(C)**, leaf trichomes **(D)**, and root **(G)** of an *ise2* seedling at 21 d after germination.
(E) An *ise2* seedling at 72 d after germination.
(F) Flower-like structure of an *ise2* seedling after 21 d.
Bars = 5 mm in **(A)** and **(E)**, 1 mm in **(B)**, **(C)**, and **(F)**, and 200 μm in **(D)** and **(G)**.

of culture (lower part of Figure 2E). Mutant seedlings often form stunted inflorescence shoot– and flower–like organs (Figure 2F) but normal-looking roots and root hairs (Figure 2G). Frequently, multiple short shoots originate from the apical dome of a single original seedling, forming a broccoli-like structure (upper part of Figure 2E). *ise2* seedlings grown in culture with 1% sucrose are sterile and perish immediately after germinating in soil or on MS medium without sucrose.

ise2 Embryos Have Branched PD

Embryonic PD resemble primary simple PD in their structure (Mansfield and Briarty, 1991). As *ise2* mutants are altered in PD-mediated cell-to-cell transport, we determined whether *ise2* PD exhibited any structural abnormalities. We processed *ise2* and wild-type embryos by high-pressure freezing/freeze substitution and analyzed the structural features of PD at several embryo developmental stages. Surprisingly, in all *ise2* embryos from late-heart to late-torpedo stages, 15% of their PD exhibited branched morphology (Figures 3B to 3D), in contrast with the single simple PD observed in wild-type embryos (Figure 3A). Branched PD were randomly distributed throughout the whole body of embryos, and no variation in their frequency was observed among late-heart, early-torpedo, and late-torpedo stages. An equally thorough transmission electron microscopy examination of different stages of *emb25* embryos revealed a similar frequency of branched PD. Fifteen percent obvious alteration in PD architecture

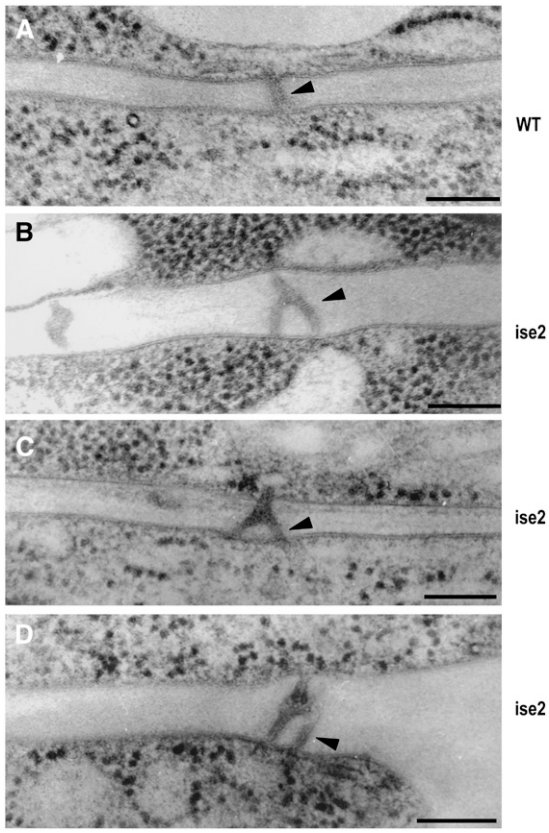

Figure 3. Micrographs of High-Pressure-Frozen/Freeze-Substituted Cotyledon Cells.

(A) Wild-type embryo. A simple PD (arrowhead) connects to adjacent cells.
(B) to **(D)** *ise2* embryos. Arrowheads point to branched PD.
Bars = 100 nm.

is highly significant. Given that *ise2* embryos have altered trafficking patterns, the remaining PD may also be altered in a manner not directly visible by transmission electron microscopy.

ISE2 Encodes a Putative DEVH Box RNA Helicase

The *ISE2* gene was isolated by positional cloning (Figure 4A) and corresponds to At1g70070, encoding a putative DEVH RNA helicase. The protein has an expected size of 132 kD and possesses all of the conserved sequences and domain motifs directly associated with RNA helicase activity (see Supplemental Figure 2 online) (de la Cruz et al., 1999). An uncharacterized mutation in this gene that affects seed pigment has been reported as *pde317* (www.seedgenes.org). The *ISE2* gene is encoded by 4181 nucleotides, with six exons interrupted by five introns (Figure 4B). A full-length cDNA clone (3564 nucleotides) was assembled from cDNA by RT-PCR amplification of the 5′ half (from ATG to the *Xho*I site at position 2522) and the 3′ half from genomic sequences without introns (from the *Xho*I site to the stop codon TAG) subcloned from the F20P5 BAC clone. Allelic tests (see Methods for details) performed by crossing heterozygous *ISE2*/*ise2* (or *emb25*/*EMB25*) plants to heterozygous *pde317* carrying a T-DNA insertion in the At1g70070 open reading frame support the positive identification of the *ise2* mutation in this predicted RNA helicase gene.

Importantly, all alleles tested, *ise2*, *emb25*, and *pde317*, showed consistently similar embryo-defective phenotypes and lack of PD aperture/SEL downregulation after the torpedo stage, determined by the F-dextran dye-loading assay (Figure 1D), comparable to those shown for *ise2* in Figure 1B. Direct sequencing of *ise2* and *emb25* genes indicated that *ise2* has a premature STOP codon at Gln-61 (CAG to TAG) and *emb25* has a change of Asp-275 to Asn (GAT to AAT) in the very conserved DEVH box (Figure 4B), which likely affects helicase function of the ISE2 protein, as analogous changes in related RNA helicases are critical for function (Cheng et al., 2005; Sengoku et al., 2006). The T-DNA insert in line *pds317* is located at the 3′ end of the last exon corresponding to the position at amino acid 904 (see seedgenes.org for more details).

Thus, all three mutations map the same gene, At1g70070, encoding a putative DEVH RNA helicase. To further confirm the identity of the *ise2* locus, we performed a complementation test. Notably, constitutive expression of the cDNA of *ISE2* fused N-terminally to GFP rescued the *emb25* phenotype. Supplemental Figure 3 online presents molecular data documenting that the transgenic rescued plant contains the expected transgenic DNA fragments in the *emb25* background. We renamed *ise2* as *ise2-1*, *emb25* as *ise2-2*, and *pde317* as *ise2-3*.

Phylogenetic analyses place the predicted ISE2 protein in the superfamily II RNA helicases, corresponding to the budding yeast Ski2p DExh RNA helicase family (de la Cruz et al., 1999). Supplemental Figure 2 online shows the high degree of homology between consensus helicase motifs between ISE2 and Ski2p. In yeast, the Ski2p RNA helicase is a main component of the Ski complex involved in the 3′ to 5′ cytoplasmic mRNA degradation pathway also found in *Drosophila* and mammalian cells (Dangel et al., 1995; Seago et al., 2001). In yeast, proteins of the Ski complex mediate degradation of mRNA by the exosome,

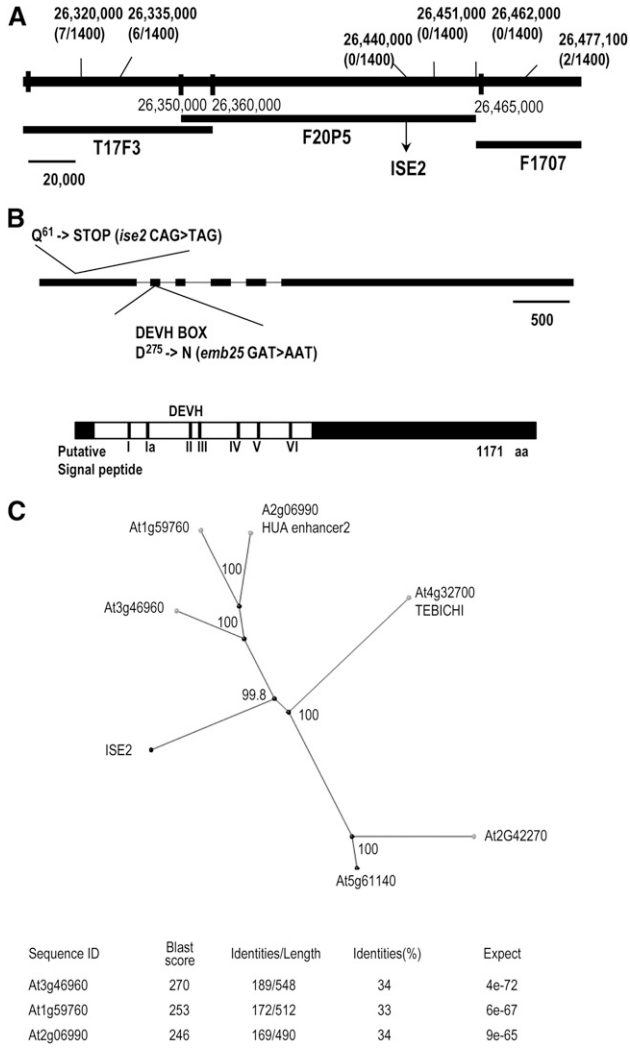

Sequence ID	Blast score	Identities/Length	Identities(%)	Expect
At3g46960	270	189/548	34	4e-72
At1g59760	253	172/512	33	6e-67
At2g06990	246	169/490	34	9e-65

Figure 4. Mapping and Cloning of the *ISE2* Gene.

(A) Genetic and molecular map of *ise2*. The frequency of recombination between PCR-based cleaved-amplified polymorphic sequence markers in a mapping population of 700 plants was scored. The least frequent recombinants (>0) were six plants with markers positioned at 26,335,000 bp and two plants with markers positioned at 26,477,100 bp. Thus, *ise2* maps to the F20P5 BAC genomic region, an interval of 100 kb predicted to contain 31 genes (At1g70220 to At1g70020; www.Arabidopsis.org). Genomic DNA sequencing from position 26,465,000 bp toward the centromere in both homozygous mutants *ise2* and *emb25* indicated single nucleotide changes at the At1g70070 locus.

(B) Top, model of the *ISE2* gene. Exons are shown as black bars. Changes in the amino acid and DNA sequences of *ise2* or *emb25* alleles are noted. The scale bar represents 500 bp. Bottom, schematic diagram of ISE2 showing the location of a putative signal peptide (small black bar), the helicase motifs within the white region, and the C-terminal region (black). aa, amino acids.

(C) Phylogenetic tree of ISE2 homologs in *Arabidopsis* using the neighbor-joining BLOSUM 62 matrix (BLASTP) and represented graphically by Jalview software. The Bootstrap statistical analyses were made with the software ClustalX using the Bootstrap Neighbor-Joining Tree function, and calculated percentage significance values are indicated in each branch. At bottom is a list of the closest *Arabidopsis* homologs with percentage amino acid identity to ISE2.

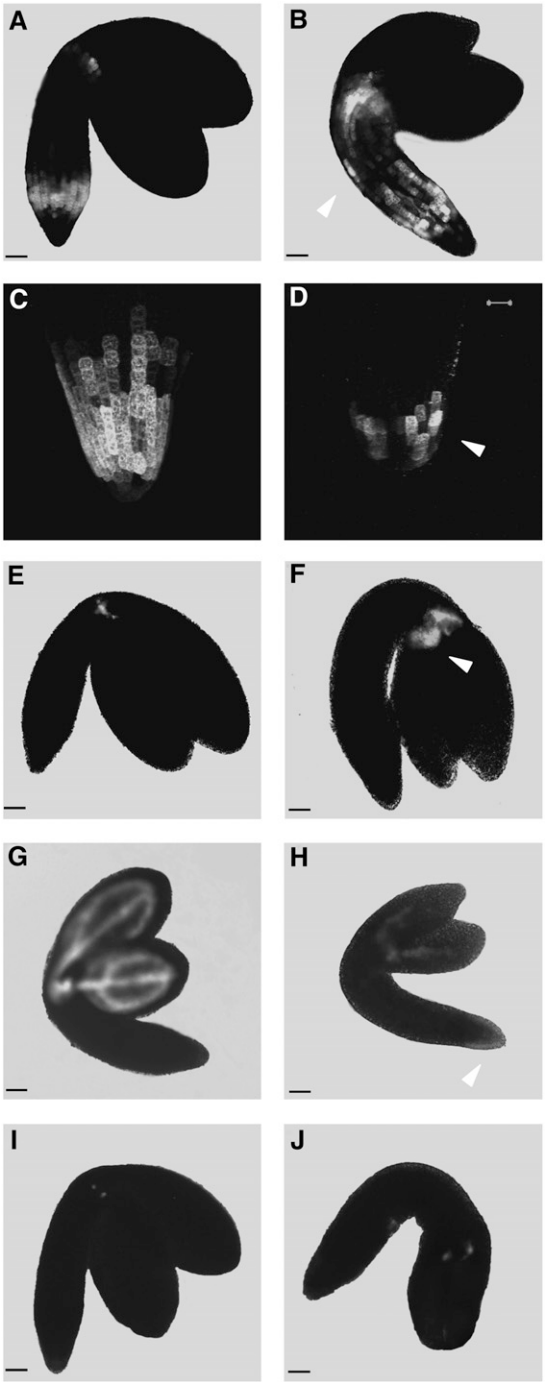

Figure 5. Expression of Cell Identity Markers during *ise2* Embryogenesis.

Wild-type embryos (**[A]**, **[C]**, **[E]**, **[G]**, and **[I]**) and *ise2* embryos (**[B]**, **[D]**, **[F]**, **[H]**, and **[J]**). Expression of the STM::ER-GFP marker line in late-torpedo stage embryos occurs in the wild-type SAM and lower hypocotyl **(A)** and ectopically in *ise2* **(B)**. The J2301 line expressing ER-GFP in the wild-type root **(C)** is reduced in the *ise2* root **(D)**. The J2341 line expresses ER-GFP at the wild-type SAM **(E)**, and broader expression, including in the basal part of cotyledons, is seen in *ise2* J2341 **(F)**. Provascular and meristem-specific expression is seen in wild-type M0164 **(G)**, and altered provascular vein pattern, no meristem expression, and ectopic root expression are seen in *ise2* M0164 **(H)**. Line M0221 expresses ER-GFP in a domain surrounding the shoot meristem in both wild-type and *ise2* embryos (**[I]** and **[J]**). Bars = 50 μm except for **(C)** and **(D)**, in which the bar (shown in **[D]**) = 20 μm. White arrowheads indicate regions of changed expression of the GFP marker in *ise2*.

a 3′ exonuclease complex (Anderson and Parker, 1998; Brown et al., 2000) (see Discussion).

In *Arabidopsis*, in addition to ISE2, the Ski2p-related RNA helicase family consists of three helicase genes: *HUA enhancer2* (*HEN2*; At2g06990), At3g46960, and At1g59760 (Figure 4C). The only member with assigned function is *HEN2*, which is required for the maintenance of B and C gene expression in the reproductive whorls and for normal spacing and number of perianth organ primordia (Western et al., 2002). The At3g46960 open reading frame is most closely related to ISE2. In global phylogenetic analyses, ISE2 shares homology with the *Oryza sativa* RNA helicase (XP_467691.1) and with *Cyanobacterium* RNA helicases (e.g., ZP_00673565.1) (see Supplemental Figure 2 online). The amino acid sequence homology between ISE2 and the At3g46960 open reading frame or yeast Ski2p is mostly confined to the conserved RNA helicase domains. However, a short region near the N terminus and the large C-terminal half outside the conserved RNA helicase domain, which together constitute almost half of ISE2, show less significant similarity to other *Arabidopsis* RNA helicases, suggesting the ISE2 helicase may have unique properties.

ISE2 transcripts are expressed at low levels and could not be detected by standard total RNA [or poly(A)-enriched mRNA] gel blot analyses. RT-PCR analyses indicated that *ISE2* transcripts are present in all organs analyzed, with slightly less abundance in the root (see Supplemental Figure 4 online). Data obtained from Genesnavigator (www.genesnavigator.com; Zimmermann et al., 2004) indicated that there is no particular organ or treatment(s) in which *ISE2* expression is induced or repressed dramatically.

Polyclonal antibody produced against the C terminus of ISE2 detected a single band of ~140 kD in total protein extracts prepared from wild-type seedlings (see Supplemental Figure 4 online) corresponding to the predicted size of the *ISE2* gene product. This 140-kD protein is absent in the *ise2-1* mutant.

Altered Expression Pattern of Cell Identity Markers during *ise2* Embryogenesis

ise2 embryos develop more slowly than wild-type embryos but do not have a severely defective body plan. We evaluated whether *ise2* embryos were affected in the cell-specific expression of several genes that are normally expressed during wild-type embryogenesis. We first crossed *ise2* heterozygous plants to a transgenic *Arabidopsis* line expressing ER-localized GFP under the control of 3.3 kb of the promoter region of *SHOOT MERISTEMLESS* (*STM*). GFP localization was monitored in wild-type and *ise2* embryos. Previously, we extensively characterized the activity of this *STM* promoter in wild-type embryos (Kim et al., 2005b). At wild-type mid- and late-torpedo stages, GFP signals were detected in the SAM and in the lower part of the hypocotyl near the root (Figure 5A). In *ise2* embryos, GFP was expressed

more extensively both below the SAM and in the entire lower half of the hypocotyl (Figure 5B).

This result prompted us to evaluate whether other cell identity markers were also misexpressed in *ise2* embryos. Haseloff GFP reporter lines (http://www.plantsci.cam.ac.uk/Haseloff/) direct tissue-specific expression of ER-GFP, due to the insertion of the GAL4 transcriptional activator coding sequence immediately downstream of cell-specific transcriptional enhancer elements. We screened the available Haseloff lines and found four that exhibit GFP expression in specific regions of the embryo. Line J2301 expresses GFP in cell files of the root epidermis (Figure 5C). Line J2341 expresses GFP in the shoot (Figure 5E) and root apical meristems (not visible in Figure 6E, but this can be seen in Kim et al., 2005a). Line M0164 expresses GFP in the procambial strands of the cotyledons (Figure 5G). Line M0221 expresses GFP in a domain surrounding the shoot meristem (Figure 5I). We crossed *ise2* heterozygous plants to each of these lines and determined the expression pattern of GFP. J2301-*ise2* mutants expressed GFP in a smaller region of the root epidermis compared with the wild type (Figure 5D). J2341-*ise2* mutants expressed GFP in a broader region near the SAM that extended into the base of the cotyledons (Figure 5F). M0164-*ise2* mutants resulted in reduced GFP expression in the procambial strands of the cotyledons (Figure 5H), likely reflecting the fact that procambial strands are not well developed in *ise2* mutants (see below). In addition, M0164-*ise2* mutants expressed GFP ectopically in the root epidermis (Figure 5H). Expression of GFP in M0221-*ise2* mutants does not appear to be affected (Figure 5J). Thus, while *ise2* embryos exhibit normal general organization of their tissues, the studies with GFP reporters suggest that the number of *ise2* cells with specific identities is reduced (exemplified by J2301-*ise2* and M0164-*ise2*) or expanded (exemplified by *STM-ise2* and J2341-*ise2*).

We monitored the expression of reporter genes at the mid-torpedo stage of development, as this is the time when we can detect a morphological distinction between *ise2* and wild-type embryos. Furthermore, this is the time when *ise2* exhibits an alteration in PD function (monitored by F-dextran transport) compared with wild-type embryos.

Supplemental Figure 5 online provides additional data to analyze one particular differentiation program, the development of leaf vein patterns. *ise2* cotyledons and first true leaves consistently exhibit aberrant vein patterns with reduced or bifurcated veins.

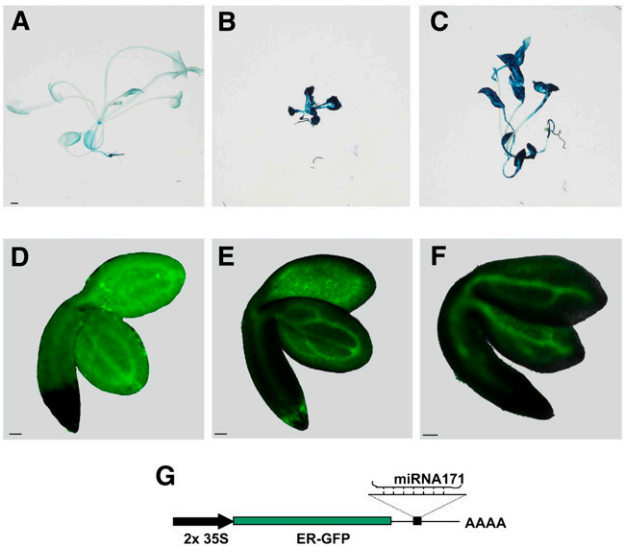

Figure 6. Gene Silencing in *ise2*.

(A) to **(C)** Effects of *sgs3-11* and *ise2-2* on posttranscriptional silencing of the L1 *35S::GUS* transgene. The wild-type L1 seedling **(A)** shows silencing of *GUS*, but *sgs3-11* **(C)** and *ise2-2* **(B)** prevent silencing in cotyledons, shoots, and leaves.

(D) to **(G)** Assay for miRNA-mediated silencing during *ise2* embryogenesis.

(D) GFP142 line (35S:ER-GFP) expressing ubiquitous ER-GFP, except in the root.

(E) Transgenic *sde1* torpedo embryo carrying the GFP171.1 construct, showing provascular GFP expression.

(F) Transgenic double mutant *sde1 ise2* torpedo embryos carrying the GFP171.1 construct showing similar provascular GFP expression.

(G) Schematic representation of the GFP171.1 construct.

Bars = 1 mm in **(A)** to **(C)** and 50 μm in **(D)** to **(F)**.

ise2 Mutants Have Decreased PTGS

Several factors influenced our decision to examine PTGS in *ise2*. First, the ISE2 putative RNA helicase shares homology with other RNA helicases participating in mRNA turnover and silencing (Figure 4) (Orban and Izaurralde, 2005). Second, mRNA turnover and RNA silencing pathways likely interact (Belostotsky, 2004; Gazzani et al., 2004). To test whether mutations in the *ISE2* predicted RNA helicase gene have an effect on transgene silencing, we crossed *ise2* to the L1 *35S::GUS* transgenic line that displays PTGS of the β-glucuronidase (GUS) reporter in fully expanded leaves and cotyledons (Elmayan et al., 1998; Peragine et al., 2004). Consistent with previous reports, crossing the *sgs3-11* mutation (which severely attenuates PTGS) into the L1 line prevented the silencing of GUS so that all leaves of the shoot display blue staining (Figure 6C) (Peragine et al., 2004). PTGS against the *GUS* gene also was suppressed in L1/*ise2* mutant seedlings germinated in vitro, resulting in intense GUS staining at hypocotyls, petioles of cotyledons, cotyledons, and true leaves (Figure 6B). GUS staining was completely absent in the original *ise2* seedling. As reported previously, wild-type L1 seedlings consistently show very weak GUS staining indicative of PTGS (Figure 6A).

Suppression of RNA silencing can result from the inhibition of short interfering RNA (siRNA) synthesis or siRNA activity (RNA-induced silencing complexes). To investigate which of these steps is inhibited in *ise2*, we determined the level of siRNA specific to GUS mRNA in the L1 background and in *ise2* in the L1 background, where it shows suppression of PTGS. Both lines produce equivalent amounts of 21-nucleotide siRNAs (Figure 7). By contrast, as reported previously, the *sgs3* mutant in the L1 background does not accumulate siRNAs (Figure 7). SGS3 protein is believed to be involved in the early steps of the silencing pathway by converting single-stranded RNA into the double-stranded RNA precursors of siRNAs (Mourrain et al.,

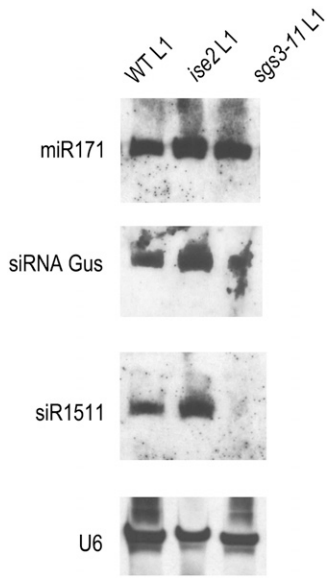

Figure 7. RNA Gel Blot Assay for Small RNAs.

miR171 RNA, siRNA specific to GUS, and ta-siR1511 were detected using oligonucleotide probes. The bottom panel shows the U6 loading control. RNA samples are from wild-type L1, *ise2*/L1, and *sgs3-11*/L1 seedlings.

2000; Dalmay et al., 2001); in support of this, SGS3 is not required for PTGS initiated by hairpin transgenes (Beclin et al., 2002).

To further characterize the role of ISE2 during RNA silencing, we assayed for the production of *trans*-acting siRNAs. SGS3 is required for the production of *trans*-acting siRNAs (Peragine et al., 2004; Yoshikawa et al., 2005), and we confirmed that *sgs3* does not produce ta-siR1511 (Figure 7). By contrast, *ise2* seedlings accumulate 21-nucleotide ta-siR1511 to wild-type levels. Thus, *ise2* does not affect the production of siRNAs or *trans*-acting siRNAs. These data together suggest that ISE2 is involved in the later steps of PTGS, potentially during siRNA-mediated degradation of target mRNAs.

MicroRNA-Mediated mRNA Downregulation Is Not Altered in *ise2*

We next evaluated whether the ISE2 predicted RNA helicase is involved in microRNA (miRNA)-mediated RNA silencing during embryogenesis. Toward this end, we obtained a transgenic line constitutively expressing a modified version of ER-GFP mRNA that contains a complementary sequence to miRNA171 in its 3′ noncoding region (Figure 6G). GFP mRNA then is degraded by the silencing pathway when and where endogenous miRNA171 is expressed (Parizotto et al., 2004). Control embryos expressing ER-GFP alone (line GFP142) showed GFP signals in the whole embryo, except in the root (Figure 6D). By contrast, torpedo embryos carrying ER-GFP fused to miRNA171 in the *sde1* background (without transitivity and secondary siRNA production) produce GFP signals most strongly in procambial region strands and cells immediately surrounding these regions (Figure 6E). The lack of GFP signals in the rest of the embryo implies that miRNA171 is expressed in these cells leading to ER-GFP mRNA degradation, analogous to that reported for adult plants (Parizotto et al., 2004). *ise2*/*sde1* embryos carrying the ER-GFP miRNA171 construct showed a similar GFP expression pattern (Figure 6F); the slight differences between wild type/*sde1* and *ise2*/*sde1* silencing reflect the altered morphogenesis and vein patterns in *ise2*. These data suggest that ISE2 does not affect miRNA171-mediated RNA silencing during embryogenesis. Together, these results imply that miRNA-induced silencing is not affected in *ise2* mutants. Furthermore, RNA gel blot analysis using a miRNA171 probe indicates that wild-type and *ise2* mutant seedlings have comparable levels of miRNA171 (Figure 7).

Subcellular Localization of ISE2

To determine the subcellular localization of the ISE2 predicted RNA helicase, we produced transgenic plants expressing ISE2 fused at its C terminus to GFP. A construct containing the entire intergenic region upstream of *ISE2* and 65 nucleotides of the coding sequence of *ISE2* placed upstream of GFP did not result in reporter gene expression. Instead, we used the 35S promoter to drive ISE2-GFP expression. As mentioned above in our complementation analyses, this version of ISE2 fully rescued the *ise2* mutant phenotype. Cauliflower mosaic virus 35S–mediated overexpression of ISE2-GFP (or ISE2) in wild-type plants did not cause major phenotypic alterations, except for slight chlorosis.

Transient expression of ISE2-GFP in *Agrobacterium tumefaciens*–infiltrated *Nicotiana benthamiana* leaves reveals GFP signal in distinct granule-like cytoplasmic structures (Figure 8A). Similarly, in transgenic ISE2-GFP *Arabidopsis*, ISE2-GFP fluorescence was found in cytoplasmic bodies often in close proximity to chloroplasts (Figure 8B). These bodies appeared to be mobile as part of cytoplasmic streaming in roots and root hairs; Figure 8C shows ISE2-GFP fluorescence in the elongated cells of the hypocotyl epidermis in transgenic ISE2-GFP *Arabidopsis*. The approximate size of the ISE2-GFP bodies is 0.2 to 0.5 μm, which is similar to the size of mitochondria observed by confocal microscopy. However, staining with Mitotracker Red indicated that ISE2-GFP localization is independent of mitochondria (Figure 8D). The homogeneity in ISE2-GFP body number per cell, size, and shape make it unlikely that they represent aggregates from overexpressing ISE2-GFP.

ISE2 Granules Are Likely SGs

The observed ISE2-specific cytoplasmic granules resemble two subcellular structures known to interact dynamically with mRNAs in yeast and mammalian cells: processing (P)-bodies and SGs (reviewed in Anderson and Kedersha, 2006; Eulalio et al., 2007). P-bodies contain components of the 5′ to 3′ mRNA decay machinery, the nonsense-mediated decay pathway, and the miRNA-induced silencing complex. Following environmental stresses such as heat, SGs accumulate mRNAs encoding many cellular proteins except for heat shock proteins. While P-bodies and SGs

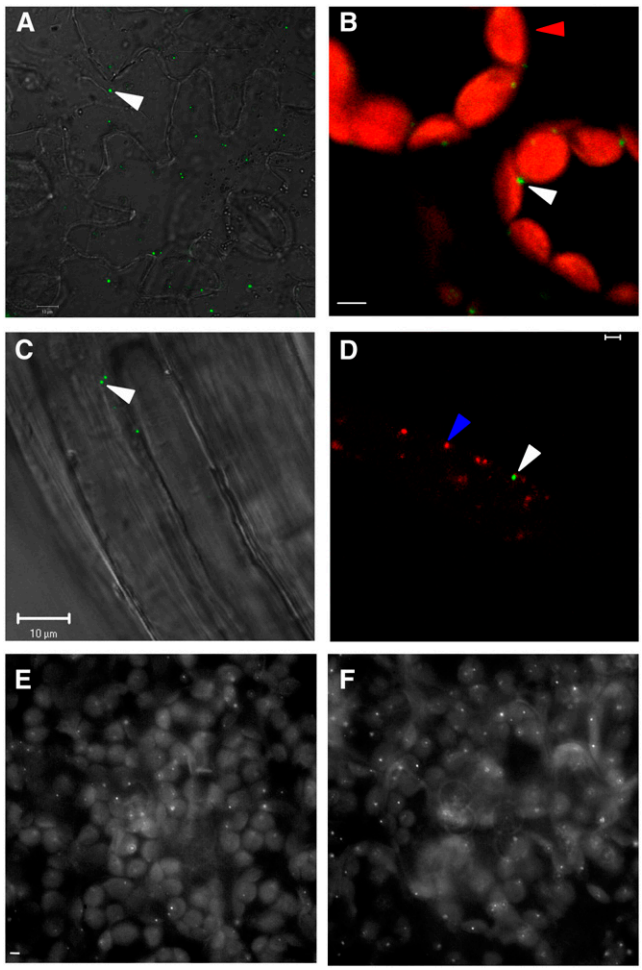

Figure 8. Subcellular Localization ISE2-GFP.

(A) *N. benthamiana* leaves agroinfiltrated with ISE2-GFP and viewed at 48 h after infection.
(B) Cotyledon cells from transgenic *Arabidopsis* seedlings showing ISE2-GFP granules compared with chloroplasts (red).
(C) Elongated hypocotyl epidermal cells from transgenic *Arabidopsis* seedlings showing ISE2-GFP granules.
(D) Root hair cell from a transgenic ISE2-GFP (green dots) *Arabidopsis* seedling stained with Mitotracker Red (red dots).
(E) and **(F)** Control **(E)** and heat shock–treated **(F)** cotyledon cells from ISE2-GFP transgenic *Arabidopsis* seedlings.
White arrowheads indicate ISE2-GFP granules, the red arrowhead indicates chloroplasts, and the blue arrowhead indicates mitochondria. Bar = 10 μm for **(A)**, **(C)**, **(E)**, and **(F)** and 2 μm for **(B)** and **(D)**.

are distinct, they share many protein components and associate with each other during stress (Teixeira et al., 2005; Wilczynska et al., 2005).

We performed a series of experiments to determine whether ISE2 might be part of a P-body or SG type of cytoplasmic RNA granule. We first evaluated ISE2 granules following heat shock treatment. Transgenic seedlings constitutively expressing ISE2-GFP were placed at 37°C for 3 to 4 h. We observed a 1.5-fold increase in the average number of ISE2-GFP granules in treated versus untreated samples; Figure 8E shows ~93 granules in control cells versus 146 granules in the heat-treated cells (Figure 8F). Supplemental Figure 6 online provides quantitative distributions of data (from 12 control and 17 heat-treated samples) illustrating that the frequency of ISE2 granules increases upon heat treatment. These results suggest that ISE2 is a SG-type cytoplasmic granule. Importantly, ISE2 granules did not aggregate even under these conditions.

Next, we tested whether ISE2 colocalizes with plant-specific markers for cytoplasmic granules. There are no plant-specific SG marker proteins identified to date. However, a recent report identifies several *Arabidopsis* P-body–specific proteins, DCP2, DCP1, and VARICOSE (Xu et al., 2006). DCP1 and DCP2 are exclusive markers of P-bodies in yeast and mammalian cells.

Figure 9 presents data obtained from two representative cells coexpressing ISE2-GFP and DCP2-RFP (for red fluorescent protein). Both cells reveal the presence of green ISE2 granules and red DCP2 granules (Figures 9A to 9F). The upper panels (Figures 9A to 9C), representing the majority of cells observed, do not reveal colocalization between ISE2 and DCP2. These data suggest that ISE2-type granules are distinct from DCP2 P-body–type granules. However, ~20% of cells analyzed (Figures 9D to 9F) revealed significant colocalization between ISE2 and DCP2.

In summary, ISE2 granules increase under heat stress and are distinct from P-bodies in ~80% of cells coexpressing ISE2 and a P-body marker protein. However, both granules can colocalize. Notably, P-bodies and SGs associate with each other in mammalian cells under oxidative stress (Kedersha et al., 2005), suggesting that the colocalization between ISE2 and P-bodies may reflect a stress response in a fraction of transfected cells.

DISCUSSION

Mutations in *ISE2* result in both functional and structural changes in PD during *Arabidopsis* embryogenesis. First, *ise2* causes an alteration in PD function, allowing continued transport of large fluorescent tracers such as 10-kD F-dextran beyond the early torpedo stage. Second, *ise2* mutants contain a highly significant number (15%) of PD with altered, branched architecture. Branched PD were observed at three developmental stages—late-heart, early-torpedo, and late-torpedo embryos—in two independent mutants, *ise2-1* and *ise2-2* (formerly *emb25*).

Molecular cloning of the *ISE2* gene reveals that it encodes a putative DEVH box RNA helicase belonging to the yeast Ski2p RNA helicase family. The ISE2 DEVH box putative RNA helicase contains all of the consensus conserved motifs for RNA helicases. Subcellular localization of ISE2-GFP reveals granule-like bodies, suggesting that ISE2 may be part of a relatively large complex. ISE2 bodies are uniform in size, suggesting that they do not result from aggregation due to overexpression.

There are numerous well-established posttranscriptional processes that regulate eukaryotic gene expression, such as mRNA degradation, translational repression, and various types of RNA-mediated gene silencing. However, it has only become apparent more recently that many of these processes occur in discrete cytoplasmic mRNA-containing particles, such as P-bodies or SGs (Anderson and Kedersha, 2006; Eulalio et al., 2007). That ISE2 also localized to discrete cytoplasmic granules prompted

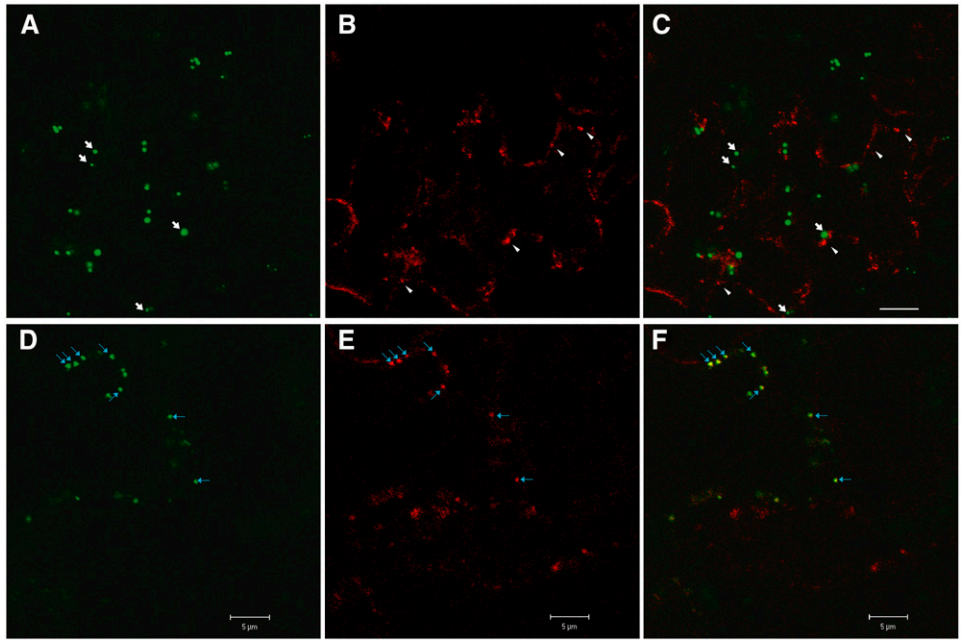

Figure 9. Subcellular Colocalization Studies of ISE2-GFP and DCP2-RFP.

N. benthamiana leaves were agroinfiltrated with ISE2-GFP and DCP2-RFP and viewed at 48 h after infection. **(A)** to **(C)** document one example of an epidermal cell with independent localization of ISE2-GFP granules (white arrows) and P-body DCP2-RFP granules (white arrowheads). DCP2-RFP exhibits a more diffuse signal. **(D)** to **(F)** show another example in which ISE2-GFP granules (green) **(D)** and the P-body DCP2-RFP granules (red) **(E)** colocalize as yellow foci **(F)**. **(A)** and **(D)** show the green GFP channel, **(B)** and **(E)** show the red RFP channel, and **(C)** and **(F)** show merged images. Blue arrows indicate colocalized granules in **(D)** to **(F)**. Bars = 10 μm for **(A)** to **(C)** and 5 μm for **(D)** to **(F)**.

us to evaluate whether ISE2 granules might be P-bodies or SGs. The data support the notion that ISE2 granules resemble SGs.

First, ISE2-granules/bodies are similar in size (~0.5 μm) to cytoplasmic granules such as SGs. Second, the ISE2 DEVH helicase is homologous to a class of helicases involved in RNA decay (Orban and Izaurralde, 2005). Third, SGs contain components participating in RNA degradation (e.g., Ago1) and translational repression, including RNA helicases (Cougot et al., 2004; Leung et al., 2006). Fourth, SGs are highly dynamic; indeed, we observed that ISE2 granules increase after a short time of exposure to heat stress. Fifth, ISE2 is involved in the PTGS pathway, as *ise2* mutants suppress gene silencing of a GUS reporter and SGs contain siRNAs involved in PTGS (Leung et al., 2006). Sixth, coexpression of ISE2 and the DCP2 P-body–specific protein reveals that ISE2 granules are distinct from P-bodies in most cells coexpressing ISE2. However, in 20% of the cells analyzed, both granules colocalized. These latter data are supported by the fact that SGs and P-bodies can share many of their components in mammalian cells (Kedersha et al., 2005; Eulalio et al., 2007).

There is precedent for other granule-associated RNA helicases in nonplant systems, such as the Rck/p54 RNA helicase that is involved in mRNA degradation and localizes to discrete P-like bodies and SGs in the cytoplasm (Eystathioy et al., 2003; Sheth and Parker, 2003; Cougot et al., 2004; Eulalio et al., 2007). The Vasa RNA helicase is a component of posterior polar granules in the developing oocyte and is required to establish the specialized translational activity of the *Drosophila* polar cytoplasm (Hay et al., 1988; Styhler et al., 2002; Cougot et al., 2004; Abdelhaleem, 2005; Chu and Rana, 2006).

Multiple sequence alignment of ISE2-related RNA helicases indicates that there are three consensus domains: an N-terminal ATP binding/RNA helicase motif that includes the DEAD/DExH box, a central helicase–C domain that is an integral part of DEAD/DExH RNA helicases, and a C-terminal DSHCT (NUC185) domain. HEN2 was the first DExH box helicase of the Ski2p family described in plants (Western et al., 2002). HEN2 shares 33% amino acid identity with ISE2; this identity is confined to central RNA helicase regions of HEN2 (71 to 525 amino acids), and HEN2 only shares 19% amino acid identity with ISE2 in the C-terminal region (526 to 991 amino acids) (Western et al., 2002). The Ski2p RNA helicase in yeast and its ortholog in *Drosophila* are the best-studied examples of helicases implicated in the cytosolic exosome RNA degradation pathway (Anderson and Parker, 1998; Orban and Izaurralde, 2005). The Ski2p helicase acts as a heterotrimer together with Ski3p and Ski8p in the exosome complex (Brown et al., 2000). In *Drosophila*, Ski2p is involved in the degradation of the 5′ mRNA product derived from miRNA-mediated mRNA cleavage (Orban and Izaurralde, 2005). Yeast and mammalian Ski2p function in the nonstop mRNA decay pathway, which prevents the translation of 3′ distal sequences in mRNAs without stop codons (Frischmeyer et al., 2002; van Hoof et al., 2002). ISE2 shares 35, 33, and 33% amino acid identity with Ski2p orthologs in human, *Drosophila*, and yeast, respectively.

Further suggestive insight for a possible role of the ISE2 putative RNA helicase in RNA processing derives from the observation that *ise2* mutants suppress transgene PTGS. Other RNA helicases are reported to be important for RNA silencing. In *Arabidopsis*, the SDE3 RNA helicase is required for the production of secondary silencing RNAs that are critical for the propagation of systemic silencing and transitivity (Dalmay et al., 2001; Himber et al., 2003). In *Chlamydomonas reinhardtii*, another DEAH box RNA helicase is necessary to degrade aberrant RNAs derived from the silencing of transposons and transgenes (Wu-Scharf et al., 2000). Exactly what role such RNA helicases play during silencing is not known. Here, we have shown that ISE2 does not affect the synthesis of 21-nucleotide siRNAs, suggesting that it acts at a later stage of the silencing pathway. Indeed, this is in agreement with a protein (such as ISE2) predicted to be involved in RNA processing and/or degradation.

If ISE2 is involved in RNA turnover, lack of the ISE2 RNA helicase may lead to the accumulation of RNAs that would normally be degraded as embryogenesis proceeds. For example, mutants of At PARN, a poly(A) 3′ to 5′ ribonuclease involved in the deadenylation of mRNA during its degradation (Reverdatto et al., 2004), are defective in the expression of a specific subset of embryo-specific transcripts. It is highly likely that messages are inappropriately expressed in *ise2*, as we observed alterations in the patterns of expression of cell identity markers exemplified in several independent GFP reporter lines. In support of this, mutation of the decapping complex proteins DCP1, DCP2, or VARICOSE in *Arabidopsis*, which also are exclusive components of P-bodies, shows severely retarded postgermination phenotypes, reflecting the fact that embryonic development was impaired (Xu et al., 2006).

To date, presumed factors that may regulate PD structure or function localize to PD such as actin, myosin, and calreticulin (reviewed in Roberts, 2005) and a recently identified kinase (Lee et al., 2005). That *ise2* embryonic PD are altered suggests that the absence of the ISE2 affects a critical factor required for correct PD formation and function.

In summary, RNA helicases act in diverse processes in gene expression, such as transcription, RNA splicing, RNA transport, RNA stability, and translation. We propose that ISE2 participates in determining the abundance of one or more mRNAs that regulate PD function and structure during *Arabidopsis* embryogenesis. Furthermore, sequence homology with RNA helicases involved in mRNA turnover, participation in PTGS, and localization to cytoplasmic SGs together indicate that ISE2 likely also represents a key player in regulating additional gene expression essential for embryo development and RNA silencing. The ISE2 helicase localized to specific granules provides an attractive probe to identify mRNAs that regulate PD function and architecture.

METHODS

Arabidopsis Growth and Transformation

Arabidopsis thaliana seeds were stratified at 4°C for 2 d, before growth at 24°C with a 16-h-light/8-h-dark cycle, either on soil or on plates with MS medium. *Agrobacterium tumefaciens* GV3101 carrying DNA constructs was used to transform *Arabidopsis* ecotype Columbia or *ISE2-2*/*ise2-2* by the floral dip method. Homozygous *ise2* seedlings were grown in MS agar supplemented with 1% sucrose. Genomic DNA was purified from 3- to 5-week-old seedlings using standard methods. The *emb25*, *pde317*, *sgs3-11*, and Haseloff enhancer trap lines were obtained from The Arabidopsis Information Resource. The L1 GUS line was a gift from Herve Vaucheret, and Olivier Voinnet kindly provided the GFP142 and GFP171.1 lines.

Isolation of *ise2*

ise2 was identified as described by Kim et al. (2002). One known mutant, *emb25* (Franzmann et al., 1995), and another, *pde317* (www.seedgenes.org), also showed a similar phenotype of increased aperture/SEL. Both were subsequently found to be allelic to *ise2* by genetic complementation.

Allelic Tests

The *ise2-1* mutants were outcrossed to wild-type Landsberg *erecta* plants twice prior to analysis. We previously established that *ise2-1* and *ise2-2* (*emb25*) are allelic (Kim et al., 2002). To test for allelism between *ise2-1* (or *ise2-2*) and the *pde317* T-DNA insertion line, the following criteria were used. When *ISE2-1*/*ise2-1* and *PDE317*/*pde317* heterozygous plants were crossed, 25% white seeds were observed among the F1 progeny seeds. This could only be only possible if these plants contained the same embryo-lethal mutations. Furthermore, phenotypically wild-type F2 plants were analyzed for the segregation patterns in their F3 progeny. As expected, some (22) selfed F2 plants contained only green seeds, and other (29) selfed F2 plants segregated 25% white seeds among F3 progeny, confirming that *ise2-1* (and *ise2-2*) are allelic to *pde317* (T-DNA insert in At1g70070).

Dye-Loading Assay

Immature seeds were placed on a glass microscope slide with 50 μL of 0.5× MS liquid culture medium containing fluorescent tracer according to the protocol described previously (Kim et al., 2002). All fluorescent probes were prepared just before assay. Embryos were released from seed coats as described previously and incubated in tracer solution for 5 min at room temperature, following by extensive washing with 0.5× MS solution. Embryos were then immediately observed by fluorescence microscopy. Wild-type embryos were always included as a control.

Subcellular Localization of ISE2-GFP and RFP-DCP2

We performed three independent agroinfiltration assays using a mixed inoculum from two *Agrobacterium* cultures harboring ISE2-GFP or RFP-DCP2 in the binary vector pMCD85. Both cultures were induced for *Agrobacterium* virulence gene expression and mixed together just prior to infiltration. Several leaves on 6 to 10 plants were infiltrated for each experiment, and expression was assayed at 48 h after infiltration by confocal microscopy. Approximately 10% of transfected cells exhibited coexpression of both constructs. Each experiment consistently resulted in 25 to 30 coexpressing cells. In total, 86 cells were analyzed in detail. In one experiment, 20% of the cells exhibited colocalization, and in the other two experiments, the colocalization frequency was 18%.

Molecular Mapping

Heterozygous wild-type/*ise2* plants (ecotype Landsberg *erecta*) were crossed to wild-type female plants of ecotype Columbia to introduce polymorphisms (Glazebrook et al., 1998). In the resulting F1 generation, 50% of plants were wild type and 50% were heterozygous for the *ise2* mutation. Heterozygous F1 plants were allowed to self, and F2 segregating populations were used for mapping. F2 plants segregated for DNA

polymorphisms between Landsberg *erecta* and Columbia as well as for the mutant phenotype. The wild type:heterozygote segregation ratio was 1:2, indicating that the mutant phenotype was the result of a single nuclear gene mutation. Homozygous wild-type F2 individuals containing the reciprocal products of meiotic recombination were used to make DNA for mapping. Mapping was achieved using cleaved-amplified polymorphic sequence markers (Lukowitz et al., 2000). Once a region containing *ise2* was defined, DNA was prepared from homozygous mutant plants, grown in culture on MS medium supplemented with sucrose, for direct genomic sequence using specific primers.

Molecular Techniques

PCR primers 5′-GTCGCCGGTTGTTCTACACT-3′ and 5′-TGAGAACA-AAACACGAAAGCA-3′, amplifying a 5′ region of *ISE2* locus containing *Bst*XI sites, were used to determine the genotype of individual plants transformed with *ISE2* cDNA. The wild-type locus contains one *Bst*XI site, giving digestion products of 341 and 181 bp, while *Bst*XI is absent in homozygous *ise2*. To analyze the expression of *ISE2* mRNA in different tissues, total RNA was extracted from quick-frozen tissue using the RNeasy plant mini kit (Qiagen), followed by digestion with DNase I (DNA-free; Ambion). Two micrograms of RNA were used as template for reverse transcription followed by PCR. C-terminal *ISE2* sequences were amplified and subsequently subcloned using pGATEWAY technology (Invitrogen). The C-terminal peptide fragment of ISE2 representing the last 320 amino acids was then expressed in *Escherichia coli* using the pDEST17 plasmid (Invitrogen), and overproduced protein was purified as inclusion bodies and inoculated into mice. Similarly, full-length *ISE2* sequences were amplified by PCR and subcloned into pMCD85 GATEWAY binary vector (Curtis and Grossniklaus, 2003) to express ISE2-GFP in plants. Primer sequences are available upon request. DCP2-RFP (Xu et al., 2006) was subcloned into the binary vector pMCD85.

Small RNA Gel Blot

Total RNA from 2-week-old seedlings was extracted using Tri-Reagent (Sigma-Aldrich) according to the manufacturer's instructions, precipitated with isopropanol, and resuspended in water for quantification. For RNA gel blot analyses, samples were electrophoresed on a 17% polyacrylamide gel containing 7 M urea in 0.5× Tris borate EDTA buffer. Probe specific for miRNA171, GUS siRNA, ta-si1511, and U6 are DNA oligonucleotides end-labeled with biotin from Operon. Hybridization was carried at 30°C using 200 mM buffer phosphate and 5% SDS. Washing and detection were done according to the Pierce's North2South chemiluminescent hybridization and detection kit instructions. Probe sequences were as follows: 5′-GATATTGGCGCGGCTCAATCA-3′ for miRNA171, 5′-AAGTATCATCATTCGCTTGGA-3′ for *trans*-acting siRNA1511, 5′-CACACTGATACTCTTCACTCCACA-3′ for GUS, and 5′-CTCTGTATCG-TTCCAATTTTATC-3′ for U6.

Light Microscopy

Seedlings and embryos were grown under greenhouse conditions and observed by epifluorescence and confocal laser scanning microscopy as described (Kim et al., 2002). Images were processed with Adobe Photoshop or Canvas 9.

Electron Microscopy

Developing wild-type and *ise2* embryos at different stages of development (from late-heart to mature embryos) were removed from their seeds, loaded in sample holders filled with a solution of 0.1 M sucrose, frozen in a Baltec HPM 010 high-pressure freezer (Technotrade), and then transferred to liquid nitrogen for storage. Substitution was performed in 2% (w/v) OsO_4 in anhydrous acetone at –80°C for 5 d, followed by slow warming to room temperature over a period of 3 d. After several acetone rinses, samples were infiltrated in Epon resin (Ted Pella) following this schedule: 10% (v/v) resin in acetone (4 h), 25% resin (12 h), and 50, 75, and 100% (24 h each concentration). Polymerization was performed at 60°C. Sections were stained with 2% uranyl acetate in 70% methanol for 10 min followed by Reynold's lead citrate (2.6% lead nitrate and 3.5% sodium citrate, pH 12) and observed with a Zeiss EM 109 microscope.

PD ultrastructure was evaluated in two late-heart, two early-torpedo, and six late-torpedo embryos. In total, ~280 PD were analyzed, and ~50 of them showed branched structure. No variation in type, frequency, or distribution was found along different stages and embryo organs.

Accession Number

The Arabidopsis Genome Initiative locus identifier for *ISE2* is At1g70070.

Supplemental Data

The following materials are available in the online version of this article.

Supplemental Figure 1. Morphological Comparison of Wild-Type and *ise2* Embryos Revealing the Enlarged SAM Region in *ise2*.

Supplemental Figure 2. Comparison of Consensus DEVH RNA Helicase Motifs with Such Motifs in ISE2 and Ski2p from Yeast, and Phylogenetic Tree of ISE2 Homologs in Diverse Organisms.

Supplemental Figure 3. The Embryo-Lethal *ise2-2* Phenotype Was Fully Rescued by Transformation with the ISE2-GFP Sequence.

Supplemental Figure 4. *ISE2* Expression Analysis.

Supplemental Figure 5. Vein Phenotypes Caused by the *ise2* Mutation.

Supplemental Figure 6. Frequency of ISE2 Granules in Control and Heat-Stressed Samples.

ACKNOWLEDGMENTS

We thank Steve Ruzin and Denise Schichnes of the Center for Biological Imaging for excellent advice on fluorescence microscopy and members of the Zambryski laboratory for constant support and critical evaluation of the experiments performed. We thank Rebecca Middleton and Kimmen Sjolander for help with phylogenetic analyses, Herve Vaucheret for line L1, Olivier Voinnet for lines GFP142 and GFP171.1, and Jun Xu and Nam-Hai Chua for DCP2-RFP DNA. K.K. thanks Fred Hempel for valuable advice on F-dextran uptake in embryos. M.S.O. expresses sincere thanks to L. Andrew Staehelin for support. S.K. and M.M. were supported by National Institutes of Health Grant PO1 HG-000205 to Ronald Davis. K.K. and P.Z. were supported by National Institutes of Health Grant GM45244.

Received July 10, 2006; revised May 29, 2007; accepted June 6, 2007; published June 29, 2007.

REFERENCES

Abdelhaleem, M. (2005). RNA helicases: Regulators of differentiation. Clin. Biochem. **38:** 499–503.

Anderson, J.S., and Parker, R.P. (1998). The 3′ to 5′ degradation of yeast mRNAs is a general mechanism for mRNA turnover that

requires the SKI2 DEVH box protein and 3′ to 5′ exonucleases of the exosome complex. EMBO J. **17:** 1497–1506.

Anderson, P., and Kedersha, N. (2006). RNA granules. J. Cell Biol. **172:** 803–806.

Beclin, C., Boutet, S., Waterhouse, P., and Vaucheret, H. (2002). A branched pathway for transgene-induced RNA silencing in plants. Curr. Biol. **12:** 684–688.

Belostotsky, D. (2004). mRNA turnover meets RNA interference. Mol. Cell **16:** 498–500.

Berleth, T., and Chatfield, S. (2002). Embryogenesis: Pattern formation from a single cell. In The Arabidopsis Book, C.R. Somerville and E.M. Meyerowitz, eds (Rockville, MD: American Society of Plant Biologists), doi/10.1199/tab.0051, http://www.aspb.org/publications/arabidopsis/.

Brown, J.T., Bai, X., and Johnson, A.W. (2000). The yeast antiviral proteins Ski2p, Ski3p, and Ski8p exist as a complex in vivo. RNA **6:** 449–457.

Cheng, P., He, Q., Wang, L., and Liu, Y. (2005). Regulation of the Neurospora circadian clock by an RNA helicase. Genes Dev. **19:** 234–241.

Chu, C.Y., and Rana, T.M. (2006). Translation repression in human cells by microRNA-induced gene silencing requires RCK/p54. PLoS Biol. **4:** e210.

Cougot, N., Babajko, S., and Seraphin, B. (2004). Cytoplasmic foci are sites of mRNA decay in human cells. J. Cell Biol. **165:** 31–40.

Crawford, K.M., and Zambryski, P.C. (2000). Subcellular localization determines the availability of non-targeted proteins to plasmodesmatal transport. Curr. Biol. **10:** 1032–1040.

Curtis, M.D., and Grossniklaus, U. (2003). A Gateway cloning vector set for high-throughput functional analysis of genes in planta. Plant Physiol. **133:** 462–469.

Dalmay, T., Horsefield, R., Braunstein, T.H., and Baulcombe, D.C. (2001). SDE3 encodes an RNA helicase required for post-transcriptional gene silencing in Arabidopsis. EMBO J. **20:** 2069–2078.

Dangel, A.W., Shen, L., Mendoza, A.R., Wu, L.C., and Yu, C.Y. (1995). Human helicase gene SKI2W in the HLA class III region exhibits striking structural similarities to the yeast antiviral gene SKI2 and to the human gene KIAA0052: Emergence of a new gene family. Nucleic Acids Res. **23:** 2120–2126.

de la Cruz, J., Kressler, D., and Linder, P. (1999). Unwinding RNA in *Saccharomyces cerevisiae*: DEAD-box proteins and related families. Trends Biochem. Sci. **24:** 192–198.

Elmayan, T., Balzergue, S., Beon, F., Bourdon, V., Daubremet, J., Guenet, Y., Mourrain, P., Palauqui, J.C., Vernhettes, S., Vialle, T., Wostrikoff, K., and Vaucheret, H. (1998). Arabidopsis mutants impaired in cosuppression. Plant Cell **10:** 1747–1758.

Eulalio, A., Behm-Ansmant, I., and Izaurralde, E. (2007). P bodies: At the crossroads of post-transcriptional pathways. Nat. Rev. Mol. Cell Biol. **1:** 9–22.

Eystathioy, T., Jakymiw, A., Chan, E.K., Seraphin, B., Cougot, N., and Fritzler, M.J. (2003). The GW182 protein colocalizes with mRNA degradation associated proteins hDcp1 and hLSm4 in cytoplasmic GW bodies. RNA **9:** 1171–1173.

Franzmann, L.H., Yoon, E.S., and Meinke, D.W. (1995). Saturating the genetic map of *Arabidopsis thaliana* with embryonic mutations. Plant J. **7:** 341–350.

Frischmeyer, P.A., van Hoof, A., O'Donnell, K., Guerrerio, A.L., Parker, R., and Dietz, H.C. (2002). An mRNA surveillance mechanism that eliminates transcripts lacking termination codons. Science **295:** 2258–2261.

Gazzani, S., Lawrenson, T., Woodward, C., Headon, D., and Sablowski, R. (2004). A link between mRNA turnover and RNA interference in Arabidopsis. Science **306:** 1046–1048.

Glazebrook, J., Drenkard, E., Preuss, D., and Ausubel, F.M. (1998). Use of cleaved amplified polymorphic sequences (CAPS) as genetic markers in *Arabidopsis thaliana*. Methods Mol. Biol. **82:** 173–182.

Goldberg, R.B., Barker, S.J., and Perez-Grau, L. (1989). Regulation of gene expression during plant embryogenesis. Cell **56:** 149–160.

Hay, B., Jan, L.Y., and Jan, Y.N. (1988). A protein component of Drosophila polar granules is encoded by vasa and has extensive sequence similarity to ATP-dependent helicases. Cell **55:** 577–587.

Himber, C., Dunoyer, P., Moissiard, G., Ritzenthaler, C., and Voinnet, O. (2003). Transitivity-dependent and -independent cell-to-cell movement of RNA silencing. EMBO J. **22:** 4523–4533.

Jurgens, G. (1995). Axis formation in plant embryogenesis: Cues and clues. Cell **81:** 467–470.

Kedersha, N., Stoecklin, G., Ayodele, M., Yacono, P., Lykke-Andersen, J., Fritzler, M.J., Scheuner, D., Kaufman, R.J., Golan, D.E., and Anderson, P. (2005). Stress granules and processing bodies are dynamically linked sites of mRNP remodeling. J. Cell Biol. **169:** 871–884.

Kim, I., Cho, E., Crawford, K., Hempel, F.D., and Zambryski, P.C. (2005a). Cell-to-cell movement of GFP during embryogenesis and early seedling development in Arabidopsis. Proc. Natl. Acad. Sci. USA **102:** 2227–2231.

Kim, I., Hempel, F.D., Sha, K., Pfluger, J., and Zambryski, P.C. (2002). Identification of a developmental transition in plasmodesmatal function during embryogenesis in *Arabidopsis thaliana*. Development **129:** 1261–1272.

Kim, I., Kobayashi, K., Cho, E., and Zambryski, P.C. (2005b). Subdomains for transport via plasmodesmata corresponding to the apical-basal axis are established during Arabidopsis embryogenesis. Proc. Natl. Acad. Sci. USA **102:** 11945–11950.

Kobayashi, K., Kim, I., Cho, E., and Zambryski, P. (2005). Plasmodesmata and plant morphogenesis. In Annual Plant Reviews, Vol. 18, K. Oparka, ed (Oxford, UK: Blackwell Publishing), pp. 90–116.

Lee, J.Y., Taoka, K., Yoo, B.C., Ben-Nissan, G., Kim, D.J., and Lucas, W.J. (2005). Plasmodesmal-associated protein kinase in tobacco and Arabidopsis recognizes a subset of non-cell-autonomous proteins. Plant Cell **17:** 2817–2831.

Lee, J.Y., Yoo, B.C., Rojas, M.R., Gomez-Ospina, N., Staehelin, L.A., and Lucas, W.J. (2003). Selective trafficking of non-cell-autonomous proteins mediated by NtNCAPP1. Science **299:** 392–396.

Leung, A.K., Calabrese, J.M., and Sharp, P.A. (2006). Quantitative analysis of Argonaute protein reveals microRNA-dependent localization to stress granules. Proc. Natl. Acad. Sci. USA **103:** 18125–18130.

Lukowitz, W., Gillmor, C.S., and Scheible, W.R. (2000). Positional cloning in Arabidopsis. Why it feels good to have a genome initiative working for you. Plant Physiol. **123:** 795–805.

Mansfield, S.G., and Briarty, L.G. (1991). Early embryogenesis in *Arabidopsis thaliana*. II. The developing embryo. Can. J. Bot. **69:** 461–476.

Mourrain, P., et al. (2000). Arabidopsis SGS2 and SGS3 genes are required for posttranscriptional gene silencing and natural virus resistance. Cell **101:** 533–542.

Oparka, K.J., Roberts, A.G., Boevink, P., Santa Cruz, S., Roberts, I., Pradel, K.S., Imlau, A., Kotlizky, G., Sauer, N., and Epel, B. (1999). Simple, but not branched, plasmodesmata allow the nonspecific trafficking of proteins in developing tobacco leaves. Cell **97:** 743–754.

Orban, T.I., and Izaurralde, E. (2005). Decay of mRNAs targeted by RISC requires XRN1, the Ski complex, and the exosome. RNA **11:** 459–469.

Parizotto, E.A., Dunoyer, P., Rahm, N., Himber, C., and Voinnet, O. (2004). In vivo investigation of the transcription, processing, endonucleolytic activity, and functional relevance of the spatial distribution of a plant miRNA. Genes Dev. **18:** 2237–2242.

Peragine, A., Yoshikawa, M., Wu, G., Albrecht, H.L., and Poethig, R.S. (2004). SGS3 and SGS2/SDE1/RDR6 are required for juvenile

development and the production of trans-acting siRNAs in Arabidopsis. Genes Dev. **18:** 2368–2379.

Reverdatto, S.V., Dutko, J.A., Chekanova, J.A., Hamilton, D.A., and Belostotsky, D.A. (2004). mRNA deadenylation by PARN is essential for embryogenesis in higher plants. RNA **10:** 1200–1214.

Roberts, A.G. (2005). Plasmodesmata structure and development. In Annual Plant Reviews, Vol. 18, K. Oparka, ed (Oxford, UK: Blackwell Publishing), pp. 1–32.

Schulz, R., and Jensen, W.A. (1968). *Capsella* embryogenesis: The egg, zygote and young embryo. Am. J. Bot. **55:** 807–819.

Seago, J.E., Chernukhin, I.V., and Newbury, S.F. (2001). The Drosophila gene twister, an orthologue of the yeast helicase SKI2, is differentially expressed during development. Mech. Dev. **106:** 137–141.

Sengoku, T., Nureki, O., Nakamura, A., Kobayashi, S., and Yokoyama, S. (2006). Structural basis for RNA unwinding by the DEAD-box protein Drosophila Vasa. Cell **125:** 287–300.

Sheth, U., and Parker, R. (2003). Decapping and decay of messenger RNA occur in cytoplasmic processing bodies. Science **300:** 805–808.

Styhler, S., Nakamura, A., and Lasko, P. (2002). VASA localization requires the SPRY-domain and SOCS-box containing protein, GUSTAVUS. Dev. Cell **3:** 865–876.

Teixeira, D., Sheth, U., Valencia-Sanchez, M.A., Brengues, M., and Parker, R. (2005). Processing bodies require RNA for assembly and contain nontranslating mRNAs. RNA **11:** 371–382.

Tzafrir, I., Pena-Muralla, R., Dickerman, A., Berg, M., Rogers, R., Hutchens, S., Sweeney, T.C., McElver, J., Aux, G., Patton, D., and Meinke, D. (2004). Identification of genes required for embryo development in Arabidopsis. Plant Physiol. **135:** 1206–1220.

van Hoof, A., Frischmeyer, P.A., Dietz, H.C., and Parker, R. (2002). Exosome-mediated recognition and degradation of mRNAs lacking a termination codon. Science **295:** 2262–2264.

West, M., and Harada, J.J. (1993). Embryogenesis in higher plants: An overview. Plant Cell **5:** 1361–1369.

Western, T.L., Cheng, Y., Liu, J., and Chen, X. (2002). HUA ENHANCER2, a putative DExH-box RNA helicase, maintains homeotic B and C gene expression in Arabidopsis. Development **129:** 1569–1581.

Wilczynska, A., Aigueperse, C., Kress, M., Dautry, F., and Weil, D. (2005). The translational regulator CPEB1 provides a link between dcp1 bodies and stress granules. J. Cell Biol. **118:** 981–992.

Wu-Scharf, D., Jeong, B., Zhang, C., and Cerutti, H. (2000). Transgene and transposon silencing in *Chlamydomonas reinhardtii* by a DEAH-box RNA helicase. Science **290:** 1159–1162.

Xu, J., Yang, J.Y., Niu, Q.W., and Chua, N.H. (2006). Arabidopsis DCP2, DCP1, and VARICOSE form a decapping complex required for postembryonic development. Plant Cell **18:** 3386–3398.

Yadegari, R., Paiva, G., Laux, T., Koltunow, A.M., Apuya, N., Zimmerman, J.L., Fischer, R.L., Harada, J.J., and Goldberg, R.B. (1994). Cell differentiation and morphogenesis are uncoupled in Arabidopsis raspberry embryos. Plant Cell **6:** 1713–1729.

Yoshikawa, M., Peragine, A., Parkm, M.Y., and Poethig, R.S. (2005). A pathway for the biogenesis of trans-acting siRNAs in Arabidopsis. Genes Dev. **19:** 2164–2175.

Zambryski, P. (2004). Cell-to-cell transport of proteins and fluorescent tracers via plasmodesmata during plant development. J. Cell Biol. **164:** 165–168.

Zimmermann, P., Hirsch-Hoffmann, M., Hennig, L., and Gruissem, W. (2004). GENEVESTIGATOR. Arabidopsis microarray database and analysis toolbox. Plant Physiol. **136:** 2621–2632.